Facile Synthesis of Graphene Quantum Dots from 3D Graphene and their Application for Fe^{3+} Sensing

*Arundithi Ananthanarayanan, Xuewan Wang, Parimal Routh, Barindra Sana, Sierin Lim, Dong-Hwan Kim, Kok-Hwa Lim, Jun Li, and Peng Chen**

Owing to their small size, biocompatibility, unique and tunable photoluminescence, and physicochemical properties, graphene quantum dots (GQDs) are an emerging class of zero-dimensional materials promising a wide spectrum of novel applications in bio-imaging, optical, and electrochemical sensors, energy devices, and so forth. Their widespread use, however, is largely limited by the current lack of high yield synthesis methods of high-quality GQDs. In this contribution, a facile method to electrochemically exfoliate GQDs from three-dimensional graphene grown by chemical vapor deposition (CVD) is reported. Furthermore, the use of such GQDs for sensitive and specific detection of ferric ions is demonstrated.

1. Introduction

Graphene is a two-dimensional monolayer of sp^2 bonded carbon atoms. Recently, 3D architectures of graphene have been employed as novel 3D electrodes for energy and sensing applications taking advantages of its highly conductive network and vast specific surface area.[1] Curving 2D graphene into 1D nanoribbon, on the other hand, can transform this zero-band semi-metal material into a semiconductor with a wide bandgap due to quantum confinement and edge effects, promising applications in nanoelectronics.[2] More recently, 0D graphene or graphene quantum dot (GQD) has been synthesized.[3] The quantum confinement influenced by the edge and defect effects renders GQDs unique and tunable photoluminescence properties, therefore, their great potentials for bio-imaging,[4] optical sensing,[5] photovoltaics,[2,6] and so forth.[7] Very recently, we have demonstrated the use of GQD as the universal fluorophore, advantageous over the conventional organic fluorophores and semiconductor QDs in several aspects, for real-time molecular tracking in live cells.[8]

A. Ananthanarayanan, X. Wang, Dr. P. Routh, Dr. B. Sana, Prof. S. Lim, Prof. D.-H. Kim, Prof. K.-H. Lim, Prof. P. Chen
School of Chemical and Biomedical Engineering
Nanyang Technological University
70 Nanyang Drive, 637457, Singapore
E-mail: ChenPeng@ntu.edu.sg

Dr. J. Li
Institute of Materials Research and Engineering
A*STAR (Agency for Science, Technology and Research)
3 Research Link, Singapore 117602, Singapore

DOI: 10.1002/adfm.201303441

GQDs can be synthesized using bottom-up or top-down approaches. The former relies on assembly of small natural or artificial cyclic molecules (e.g., hexa-peri-hexabenzocoronene, polyphenyls) with good control of the size, shape and properties of the resulting GQDs size.[9] These approaches, however, often suffer from tedious and challenging synthetic procedures and poor yield. The top-down methods, on the other hand, involve exfoliation and break-down from various carbon materials (e.g., carbon fibers,[10]graphite rods,[11]carbon black,[4a] carbon nanotubes,[12] graphene oxide)[13][3,14] using solvothermal, hydrothermal, mechanical, chemical and electrochemical means. These methods, however, usually are of low throughput and produce GQDs with non-ideal or non-uniformly distributed lateral size and thickness (layer number).[11b] And the harsh synthetic process inevitably damages the graphene lattice. Intuitively, direct scissoring from defect-free graphene would ensure high-yield and high-quality of GQDs.

Herein, we report a new electrochemical strategy for facile synthesis of high quality GQDs from monolithic 3D graphene grown by chemical vapour deposition (CVD) (**Figure 1**). And as a proof of-concept demonstration, the obtained GQDs are employed for specific detection of iron ions (Fe^{3+}).

2. Results and Discussion

3D graphene is grown by chemical vapour deposition (CVD) as reported previously.[15] It is a monolithic macroporous structure (**Figure 2**a) of interconnected defect-free graphene network consisting of mainly single- or few-layer domains (evidenced by the absence of defective Raman D band and the intensity ratio of 2D and G bands as shown in Figure 2c). Electrochemical route has been applied to carve out carbon nanoparticles and nanoribbons from graphite rod.[11b] Here, we electrochemically incise the free-standing 3D graphene to produce GQDs, using room temperature ionic liquid (1-butyl-3-methylimidazolium hexafluorophosphate($BMIMPF_6$) in acetonitrile) as the electrolyte which gives high ionic conductivity and wide electrochemical potential window. We have attempted different protocols and found that applying a constant voltage of 5 V for 100 s gives high yield of GQDs while achieving uniform etching of graphene foam and preserving its 3D structure (see also Figure S1 in Supporting Information). The voltage and time required for

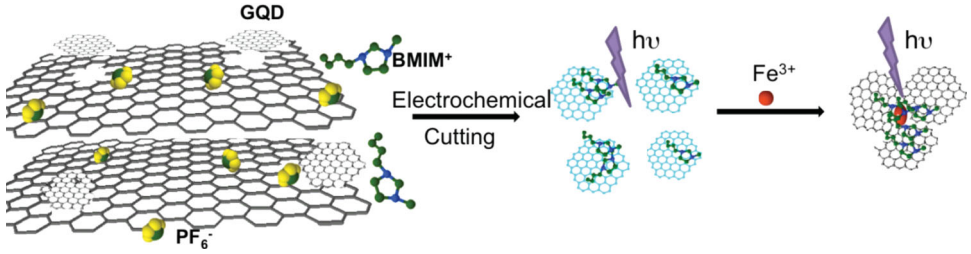

Figure 1. Schematic illustration of GQD synthesis from 3D graphene and mechanism of Fe^{3+} detection.

synthesis is lower than the methods reported by Lu et al. (6–8V, 240 min)[11b] and Zhang et al.[11a] (180 min), where exfoliation of graphite rods was carried out. During the electrochemical etching, the colourless electrolyte solution quickly turns into dark brown due to rapid flaking-off of abundant GQDs. After etching (for 100s), pinholes are created uniformly on the graphene skeleton and the defect-activated Raman D and D+D' bands arise as expected Figure 2c.

We propose that the mechanism of electrochemical cutting (Figure 1) is attributable to: 1) high electrical stress by the applied voltage; 2) the ability of PF_6^- to intercalate between the graphene layers;[11b] 3) intimate interaction (pi-pi or cation-pi interaction) between $BMIM^+$ group and GQD.[11b] As shown by Fourier transform infrared spectroscopy (FTIR), the obtained GQDs exhibit the triplet characteristic peaks of C–H asymmetric and symmetric vibration (at 2960, 2921, and 2852 cm^{-1}),[16] presumably originated from the alkyl groups of $BMIM^+$ albeit with a slight shift (Figure 2d). In addition, X-ray photoelectron spectroscopy (XPS) demonstrates several characteristic peaks corresponding to the binding energies of C–C/C = C, (C–)C–N, C = C-N and N–C = N bonds, in addition to the prominent C–C/C = C peak (Figure 2e). This observation confirms the hybridization between GQD and $BMIM^+$. We also found that, comparing to other ionic liquids (including 1-Butyl-3-Methyl Imidazolium chloride (BMIMCl), tetra ethyl ammonium chloride (TEAC), $BMIMPF_6$ gives the highest yield. Furthermore, we found that tetrabutylammonium hexafluorophosphate ($TBAPF_6$) can also effectively exfoliate GQDs from 3D graphene, suggesting the facilitating role of PF_6^- ions in cleaving graphene substrate. $BMIM^+$, on the other hand, assists to disperse GQDs in both, organic solvents and water due to its amphiphilic property. The GQD aqueous dispersions are highly stable (no obvious aggregation observed for months). We have attempted the same protocol for 2D CVD-grown graphene.

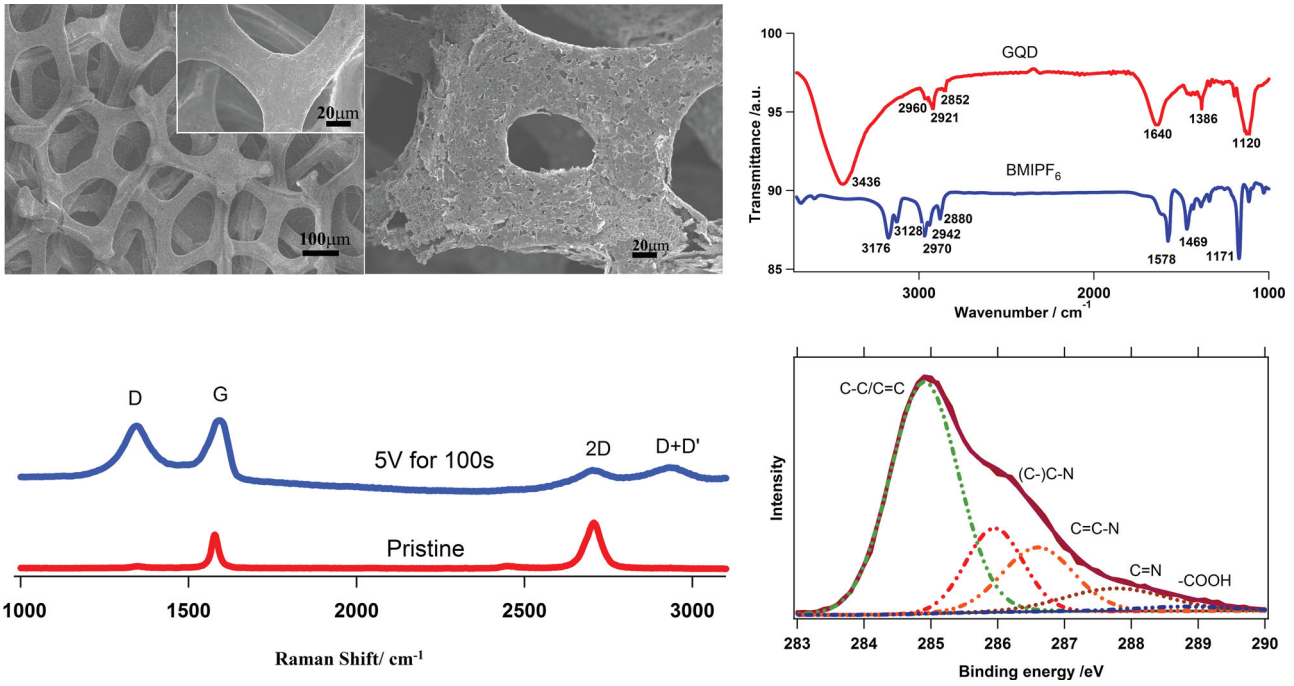

Figure 2. SEM images of 3D graphene a) before and b) after electrochemical treatment. The inset in (a) shows the surface of graphene skeleton at a higher magnification. c) Raman spectra of 3D graphene before and after electrochemical treatment. d) FTIR Spectra of GQDs and $BMIMPF_6$. e) XPS spectrum of GQDs.

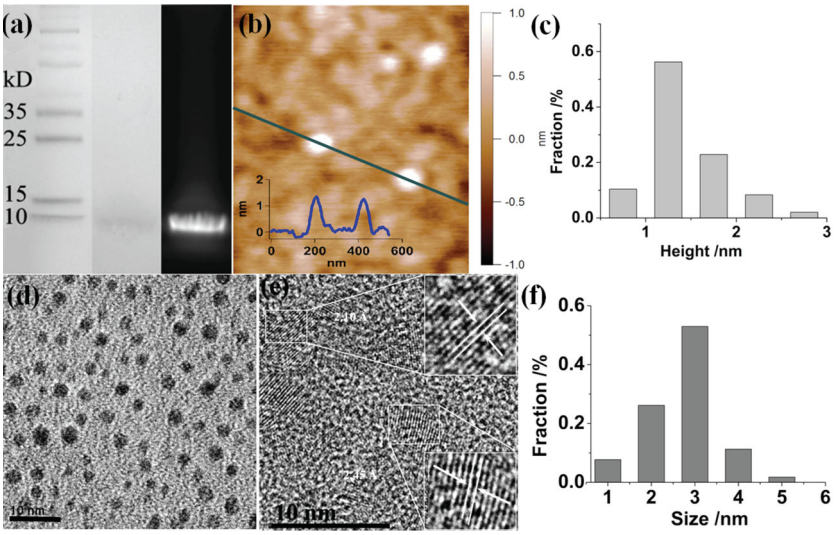

Figure 3. a) Electrophoresis gel image of GQD samples. b) AFM image of GQDs. The inset shows the height profile along the indicated line. c) Height distribution obtained from AFM measurements (203 samples). d,e) TEM images of GQDs. The insets show the lattice spacing of GQDs. f) Diameter distribution obtained from TEM images (166 samples).

But unlike 3D graphene which serves as a macroscopic free-standing electrode, 2D graphene film quickly disintegrates leading to electrical discontinuity and poor yield of GQDs.

Gel electrophoresis (SDS-PAGE) of GQDs indicates that the obtained GQDs are narrowly distributed in size and of low molecular weight as evidenced by the narrow electrophoretic band below the band of 10 kDa protein marker (**Figure 3**a). The atomic force microscopy (AFM) reveals that the average thickness of GQDs is ≈1.25 nm, indicating that they are mostly single-layered (note that the attached $BMIM^+$ groups contribute to the measured thickness) (Figure 3b,c). And as revealed by transmission electron microscopy (TEM), the GQDs have an average lateral diameter of 3.0 nm with a narrow size distribution (Figure 3d–f). The graphitic lattice of GQD can be clearly resolved under high-resolution TEM (Figure 3e). The observed two kinds of lattice spacing (2.10 Å and 2.45 Å) correspond to the hexagonal lattice plane spacing of d_{1100}[13] and d_{1120},[4c] respectively. Evidently, the produced GQDs are uniform and of high crystallinity.

GQD dispersion appears light-brown under day light and emits blue fluorescence under UV (365 nm) (**Figure 4**a, inset). Similar to the GQDs prepared by other methods, ours efficiently absorb UV light (Figure 4a). π–π* transition of aromatic sp^2 domains is reported to be responsible for the strong UV absorption below 300 nm.[17] The UV excitation spectrum exhibits two peaks (at 243 nm and 360 nm) corresponding σ–π and π–π* transitions originated from the carbene like triplet state of the zig-zag edges of GQDs (Figure 4a).[2] Excitation dependent emission is observed as the excitation wavelength varies from 300 to 500 nm (Figure 4b). The maximum emission intensity from GQDs is achieved at 440 nm when excited at 360 nm. A quantum yield of about 10% at pH 7 is calculated using quinine sulfate as the reference, which is higher than that of the previously reported GQDs electrochemically exfoliated from graphite.[11] This higher quantum yield could be attributed to the high crystallinity of GQDs and the presence of $BMIM^+$ on GQD surface which bears electron-withdrawing nitrogen groups.[18] The electrochemical band gap of GQDs is estimated to be ≈2.17 eV (Figure S2 in Supporting Information).

As GQDs are emerging as a new class of fluorescent sensors owing to its unique optical properties, small size, good solubility, photostability, chemical inertness, and biocompatibility,[5,7,8,19] we speculated that $BMIM^+$ functionalized GQDs may be employed to optically detect Fe^{3+} as it is known the imidazole ring of $BMIM^+$ has a high binding affinity to ferric ions (Fe^{3+}).[20] Fe^{3+} ions play important roles in biological systems by complexation with various regulatory proteins.[21] On the other hand, excess Fe^{3+} ions can lead to over-production of free radicals hence cytotoxicity. High Fe^{3+} concentration in neurons is also a key marker for Parkinson's disease.[21] Therefore, detection of Fe^{3+} ions in biological systems as well as its environmental monitoring is important.

GQDs fluoresce well over a wide pH range. But GQD fluorescence decreases with increasing pH because high pH attenuates GQD's interaction with $BMIM^+$ whose pyridinic nitrogen can enhance the fluorescence by imposing n-doping like characteristics to GQD (**Figure 5**a).[18] Also as shown (Figure 5a), the presence of Fe^{3+} ions (200 μM) causes significant quenching of GQD fluorescence. And the quenching is most prominent at pH 4, which is thus chosen for the following experiments. It is conceivable that Fe^{3+} ion acts as a coordinating centre to bridge several $BMIM^+$-functionalized GQDs together and quenching occurs from the induced aggregation of GQDs (Figure 1).[22] Furthermore, the fluorescence quenching of GQDs is highly selective to Fe^{3+} (68% quenching upon addition of 400 μM Fe^{3+}) while other metal ions (Mg^{2+}, Fe^{2+}, Zn^{2+}, Co^{2+}, Ni^{2+}, Cd^{2+}, and K^+)

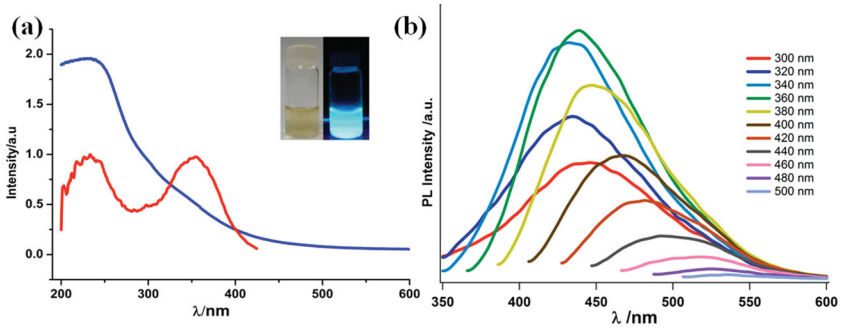

Figure 4. a) UV-vis absorption (blue) and excitation (red) spectra of GQDs. The inset shows the photographs of aqueous dispersions of GQDs under day light (left) and UV (365 nm) illumination (right). b) PL spectra of GQD solution under different excitation wavelength.

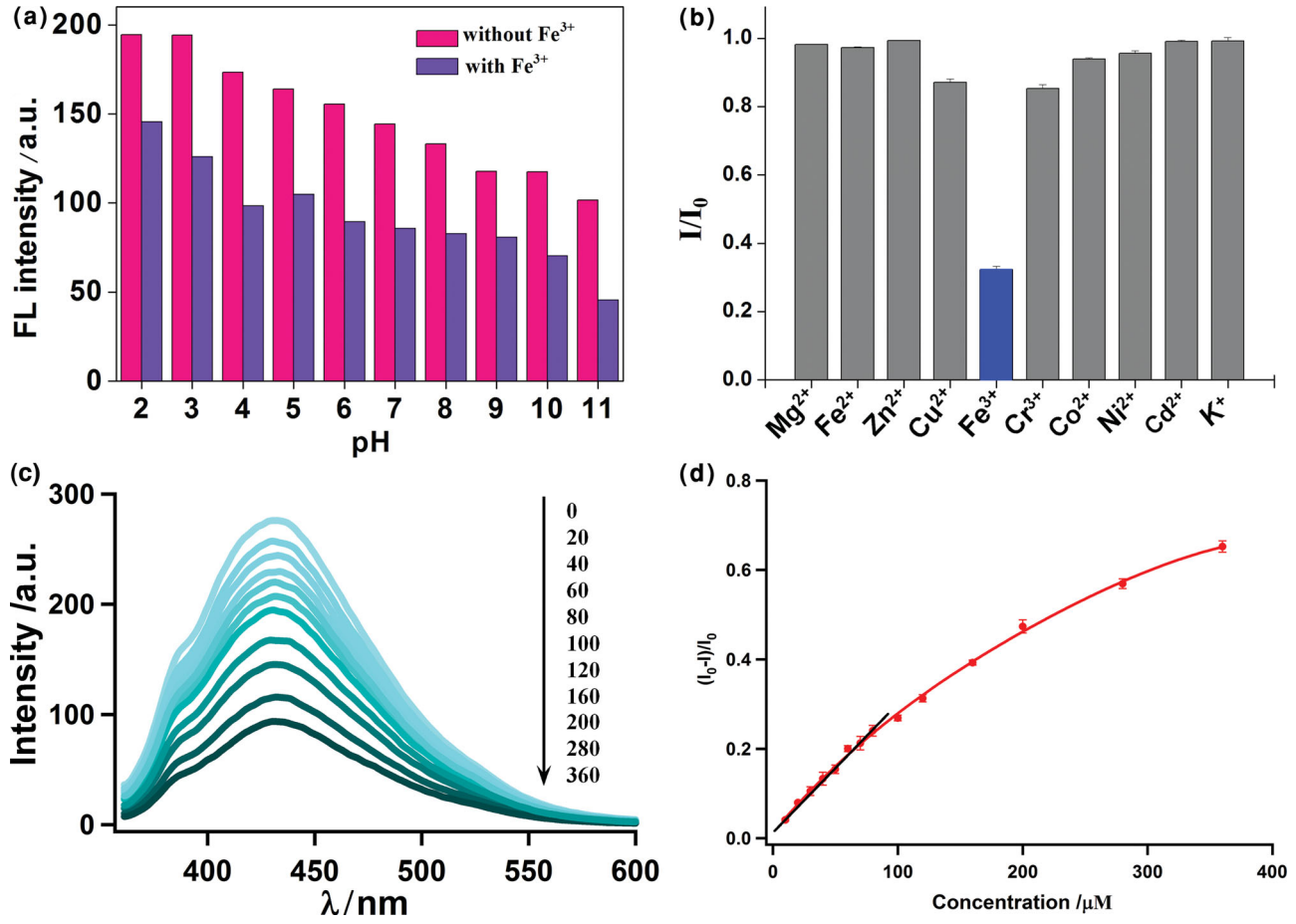

Figure 5. a) PL of GQDs (50 μg mL^{-1}) in the absence (red) and presence (purple) of 200 μM Fe^{3+} at different pH. b) Remaining percentage of GQD PL after addition of different metal ions (400 μM) in acetate buffer solution (pH 4.0). c) PL emission spectra of GQDs in the presence of Fe^{3+} ions at different concentrations (μM). The arrow indicates the change of concentration. d) Average concentration-dependent fluorescence response in the acetate buffer solution. The error bars indicate the standard deviations ($n = 3$). Linear fitting is performed in the low concentration range (black line).

are not able to exert significant quenching effect (Figure 5b). As shown in Figure 5c, the fluorescence quenching by Fe^{3+} is dose dependent, and the response spans over a wide concentration range with a theoretical lower detection limit of ≈ 7.22 μM (= $3\sigma/m$ where σ is the standard deviation, m is the slope of the linear response region at low concentrations less than 80 μm) (Figure 5d).

Fe^{3+} induced aggregation of GQDs is confirmed by AFM measurements (Figure S3 in Supporting Information) and particle size measurement based on dynamic light scattering. GQD aggregates are few-layered and 10.425 ± 4.275 nm in diameter. We speculated that such small Fe^{3+}-containing particles may serve as contrast agents for magnetic resonance imaging (MRI). As shown in Table S1 in Supporting Information, these particles indeed exhibit good magnetic response as evidenced by much lowered spin-spin relaxation time (T2) as compared to the pure GQD samples at the same concentration. We further speculated that the electrochemically-etched (yet still monolithic) 3D graphene skeleton may serve as a good electrochemical electrode because of the numerous defects and edges created by the exfoliation that are able to facilitate electron transfer, its large surface area, and its continuous multiplexed conduction network.[1b] Indeed, as demonstrated in (Figure S4 in Supporting Information), the electrochemical response of the electrochemically treated 3D graphene (to redox species ferricyanide as an example) is greatly higher than that of the bare 3D graphene or the standard 2D glassy carbon electrode.

3. Conclusions

In summary, we have developed a highly efficient and "green" electrochemical strategy to synthesize GQDs from 3D CVD-graphene with high throughput. The synthesized GQDs are of high crystallinity and uniform distribution in lateral diameter (≈3 nm) and thickness (mostly single-layered). Furthermore, the electrochemically etched graphene foam can serve as a superior 3D electrochemical electrode than bare 3D graphene. The ionic liquid used in the synthetic process not only assists in exfoliation and dispersion of GQDs but also endows GQDs with the ability for sensitive and specific optical detection of Fe^{3+} ions. In addition, the magnetic property of the

Fe^{3+}-induced GQD aggregates may promise other applications (e.g., for MRI imaging). We also envision that the versatility of this synthesis approach permits synthesis of GQDs with tailored functionalities by varying the used solvent or electrolyte and tuning the etching protocol. This development would pave the way for the widespread applications of such emerging zero-dimensional materials in various fields.

4. Experimental Section

Materials: All chemicals were purchased from Sigma Aldrich (Singapore). Nickel foam was purchased from Alantum Advanced Technology Materials. Dialysis membranes were purchased from Spectra/Pro Biotec.

3D Graphene Synthesis: As previously reported,[15] 3D graphene was synthesized by chemical vapour deposition (CVD) using nickel foam (2 mm thick, Alantum Advanced Technology Materials) as the growth substrate and ethanol as the carbon source. Nickel foam was subsequently removed with 3 M HCl at 60 °C, leaving graphene foam free-standing. After thorough rinsing with DI water and drying in oven at 50 °C, 3D graphene (cut into 0.6 cm × 1 cm) was mounted onto a glass slide. Finally, an electrode is fabricated by making an electrical lead from one end of graphene substrate using silver paint and a copper wire (insulated by silicon rubber).

Synthesis of GQDs: Using 1-Butyl-3-methylimidazolium hexafluorophosphate ($BMIMPF_6$) in acetonitrile (10%, v/v) as the electrolyte, a constant voltage or a cyclic voltage waveform was applied to 3D graphene using a CHI 660D electrochemical workstation (Chenhua) with a platinum wire as the counter electrode and an Ag/AgCl electrode as the reference. After the electrochemical exfoliation, the resultant GQD solution was centrifuged at 6000 rpm for 20 min to remove large particles, and then diluted with DI water (1/20, v/v). Acetonitrile was removed by rotary evaporator at 55 °C. GQD solution was then dialyzed with cellulose ester dialysis membrane (MWCO 500–1000D) for 3 days to completely remove the electrolyte. Finally, GQD solution was ultrafiltrated using a centrifugal filter device with a molecular-weight-cut-off at 3000 Da.

Characterization: The 3D graphene was examined by field-emission scanning electron microscopy (JSM6700-FESEM, JEOL). GQDs were inspected by atomic force microscopy (MFP-3D AFM microscope, Asylum research) and high-resolution transmission-electron microscope (HRTEM, JEOL 2010) at an accelerating voltage of 200 kV. Raman spectra were recorded using WITeck CRM200 Raman System, with laser excitation wavelength of 514 nm. Fourier transform infrared spectroscopy (FTIR) and X-ray photoelectron spectroscopy (XPS) measurement were conducted with PerkinElmer Spectrum GX FTIR system and ESCALAB MK II X-ray photoelectron spectrometer, respectively. SDS-PAGE (12%) was conducted using Mino-Protean Tetra Cell (Bio-Rad) to investigate the molecular weight distribution of prepared GQD sample. Spectra Multicolor Broad Range Protein Ladder (ThermoScientific) was employed as the molecular weight marker. The UV-vis absorption and photoluminescence spectrum of GQDs was characterized by UV-2450 spectrophotometer (Shimadzu) and LS-55 fluorescence spectrometer (PerkinElmer), respectively. Particle size of Fe^{3+}-induced GQD aggregations was measured using Zetasizer (Malvern Instruments). For magnetic characterization, samples were scanned in a 3.0 Tesla whole body scanner (Magnetom Verio, Siemens) using a dedicated knee coil.

Supporting Information

Supporting Information is available from the Wiley Online Library or from the author.

Acknowledgements

A.A. and X.W. contributed equally to this work. This work was supported by the Singapore Ministry of Education under the AcRF Tier 2 grant (MOE2011-T2–2–010).

Received: October 7, 2013
Revised: November 27, 2013
Published online: January 27, 2014

[1] a) Y. C. Yong, X. C. Dong, M. B. Chan-Park, H. Song, P. Chen, *ACS Nano* **2012**, *6*, 2394; b) Y. Liu, X. Dong, P. Chen, *Chem. Soc. Rev.* **2012**, *41*, 2283; c) X. C. Dong, X. W. Wang, L. H. Wang, H. Song, H. Zhang, W. Huang, P. Chen, *ACS Appl. Mater. Interfaces* **2012**, *4*, 3129.

[2] Y. Li, Y. Hu, Y. Zhao, G. Q. Shi, L. E. Deng, Y. B. Hou, L. T. Qu, *Adv. Mater.* **2011**, *23*, 776.

[3] D. Pan, J. Zhang, Z. Li, M. Wu, *Adv. Mater.* **2010**, *22*, 734.

[4] a) Y. Q. Dong, C. Q. Chen, X. T. Zheng, L. L. Gao, Z. M. Cui, H. B. Yang, C. X. Guo, Y. W. Chi, C. M. Li, *J. Mater. Chem.* **2012**, *22*, 8764; b) Q. Liu, B. Guo, Z. Rao, B. Zhang, J. R. Gong, *Nano Lett.* **2013**, *13*, 2436; c) J. Peng, W. Gao, B. K. Gupta, Z. Liu, R. Romero-Aburto, L. H. Ge, L. Song, L. B. Alemany, X. B. Zhan, G. H. Gao, S. A. Vithayathil, B. A. Kaipparettu, A. A. Marti, T. Hayashi, J. J. Zhu, P. M. Ajayan, *Nano Lett.* **2012**, *12*, 844; d) W. J. Xie, Y. Y. Fu, H. Ma, M. Zhang, L. Z. Fan, *Acta Chim. Sin.* **2012**, *70*, 2169; e) M. M. Xie, Y. J. Su, X. N. Lu, Y. Z. Zhang, Z. Yang, Y. F. Zhang, *Mater. Lett.* **2013**, *93*, 161; f) S. J. Zhu, J. H. Zhang, S. J. Tang, C. Y. Qiao, L. Wang, H. Y. Wang, X. Liu, B. Li, Y. F. Li, W. L. Yu, X. F. Wang, H. C. Sun, B. Yang, *Adv. Funct. Mater.* **2012**, *22*, 4732.

[5] a) J. M. Bai, L. Zhang, R. P. Liang, J. D. Qiu, *Chem. Eur. J.* **2013**, *19*, 3822; b) Y. H. Li, L. Zhang, J. Huang, R. P. Liang, J. D. Qiu, *Chem. Commun.* **2013**, *49*, 5180; c) H. M. Zhao, Y. Y. Chang, M. Liu, S. Gao, H. T. Yu, X. Quan, *Chem. Commun.* **2013**, *49*, 234; d) J. J. Liu, X. L. Zhang, Z. X. Cong, Z. T. Chen, H. H. Yang, G. N. Chen, *Nanoscale* **2013**, *5*, 1810; e) L. S. Fan, Y. W. Hu, X. Wang, L. L. Zhang, F. H. Li, D. X. Han, Z. G. Li, Q. X. Zhang, Z. X. Wang, L. Niu, *Talanta* **2012**, *101*, 192; f) Y. Q. Dong, G. L. Li, N. N. Zhou, R. X. Wang, Y. W. Chi, G. N. Chen, *Anal. Chem.* **2012**, *84*, 8378; g) H. Sun, L. Wu, W. Wei, X. Qu, *Mater. Today* **2013**, *16*, 433.

[6] V. Gupta, N. Chaudhary, R. Srivastava, G. D. Sharma, R. Bhardwaj, S. Chand, *J. Am. Chem. Soc.* **2011**, *133*, 9960.

[7] Z. P. Zhang, J. Zhang, N. Chen, L. T. Qu, *Energy Environ. Sci.* **2012**, *5*, 8869.

[8] X. T. Zheng, A. Than, A. Ananthanaraya, D. H. Kim, P. Chen, *ACS Nano* **2013**, *7*, 6278.

[9] a) X. Yan, B. Li, L. S. Li, *Acc. Chem. Res.* **2012**, *46*, 2254; b) R. L. Liu, D. Q. Wu, X. L. Feng, K. Mullen, *J. Am. Chem. Soc.* **2011**, *133*, 15221.

[10] J. Peng, W. Gao, B. K. Gupta, Z. Liu, R. Romero-Aburto, L. Ge, L. Song, L. B. Alemany, X. Zhan, G. Gao, S. A. Vithayathil, B. A. Kaipparettu, A. A. Marti, T. Hayashi, J. J. Zhu, P. M. Ajayan, *Nano Lett.* **2012**, *12*, 844.

[11] a) M. Zhang, L. L. Bai, W. H. Shang, W. J. Xie, H. Ma, Y. Y. Fu, D. C. Fang, H. Sun, L. Z. Fan, M. Han, C. M. Liu, S. H. Yang, *J. Mater. Chem.* **2012**, *22*, 7461; b) J. Lu, J.-x. Yang, J. Wang, A. Lim, S. Wang, K. P. Loh, *ACS Nano* **2009**, *3*, 2367.

[12] a) D. B. Shinde, V. K. Pillai, *Chem. Eur. J.* **2012**, *18*, 12522; b) L. Lin, S. Zhang, *Chem. Commun.* **2012**, *48*, 10177.

[13] S. H. Jin, D. H. Kim, G. H. Jun, S. H. Hong, S. Jeon, *Acs Nano* **2013**, *7*, 1239.

[14] a) F. Liu, M.-H. Jang, H. D. Ha, J.-H. Kim, Y.-H. Cho, T. S. Seo, *Adv. Mater.* **2013**, *25*, 3657; b) J. Lu, M. Yan, L. Ge, S. Ge, S. Wang,

J. Yan, J. Yu, *Biosens. Bioelectron.* **2013**, *47*, 271; c) S. Zhuo, M. Shao, S. T. Lee, *ACS Nano* **2012**, *6*, 1059; d) X. Zhou, Y. Zhang, C. Wang, X. Wu, Y. Yang, B. Zheng, H. Wu, S. Guo, J. Zhang, *ACS Nano* **2012**, *6*, 6592.

[15] X. C. Dong, Y. F. Cao, J. Wang, M. B. Chan-Park, L. H. Wang, W. Huang, P. Chen, *RSC Adv.* **2012**, *2*, 4364.

[16] a) J. Grondin, J.-C. Lassègues, D. Cavagnat, T. Buffeteau, P. Johansson, R. Holomb, *J. Raman Spectrosc.* **2011**, *42*, 733; b) H. Yang, C. Shan, F. Li, D. Han, Q. Zhang, L. Niu, *Chem. Commun.* **2009**, 3880.

[17] Y. Li, Y. Zhao, H. Cheng, Y. Hu, G. Shi, L. Dai, L. Qu, *J. Am. Chem. Soc.* **2012**, *134*, 15.

[18] Q. Li, S. Zhang, L. Dai, L. S. Li, *J. Am. Chem. Soc.* **2012**, *134*, 18932.

[19] a) H. Razmi, R. Mohammad-Rezaei, *Biosens. Bioelectron.* **2013**, *41*, 498; b) L. Zhang, Y. Xing, N. He, Y. Zhang, Z. Lu, J. Zhang, Z. Zhang, *J. Nanosci. Nanotechnol.* **2012**, *12*, 2924; c) Y. Zhang, C. Wu, X. Zhou, X. Wu, Y. Yang, H. Wu, S. Guo, J. Zhang, *Nanoscale* **2013**, *5*, 1816.

[20] N. Bian, Q. Chen, X. L. Qiu, A. D. Qi, B. H. Han, *New J. Chem.* **2011**, *35*, 1667–1671.

[21] J. L. Beard, *J. Nutr.* **2001**, *131*, 568S.

[22] J. M. Bai, L. Zhang, R. P. Liang, J. D. Qiu, *Chemistry* **2013**, *19*, 3822.